Erciyes University Journal of Institute Of Science and Technology

Research Article
10.65520/erciyesfen.1937198

Imprint:
Volume: 42(2)
Year: 2026
Page: 739-759

Comparative Performance Analysis of an SMA-Optimized FOPID Controller for an Inverted Pendulum on a Cart

Merve TÜRKTAM[a*]
Selim SOYLU[b]
Hasan ZORLU[c]

[a] PhD. Student, Erciyes University, merveturktam@yyu.edu.tr
[b] Asst. Prof., Aksaray University, selimsoylu@aksaray.edu.tr
[c] Asst. Prof., Erciyes University, hzorlu@erciyes.edu.tr

[*] Corresponding Author

Received: 4/24/2026
Accepted: 7/6/2026

Citation:
Merve TÜRKTAM, Selim SOYLU, Hasan ZORLU (2026). Comparative Performance Analysis of an SMA-Optimized FOPID Controller for an Inverted Pendulum on a Cart. *Erciyes University Journal of Institute Of Science and Technology*, 42(2), 739-759.
https://doi.org/10.65520/erciyesfen.1937198

Screened by iThenticate for Authors & Researchers

Except where otherwise noted, content in this article is licensed under a Creative Commons 4.0 International license. Icons by Font Awesome.

Abstract

This study investigates the tuning of a Fractional-Order Proportional-Integral-Derivative (FOPID) controller for a cart–inverted pendulum system, which is an inherently nonlinear and unstable system requiring simultaneous stabilization of the pendulum angle and regulation of the cart position. Although various optimization methods have been widely employed in the literature for this problem, the performance of the Slime Mould Algorithm (SMA) in the context of inverted pendulum control has not been sufficiently investigated. Motivated by this gap, the five parameters of the controller were determined using SMA, Grey Wolf Optimization (GWO), and Artificial Hummingbird Algorithm (AHA), and all methods were comparatively evaluated under identical simulation conditions based on the Integral Time Absolute Error (ITAE) criterion. The obtained results demonstrate that the SMA-based design yields lower ITAE variability and higher repeatability compared to the other methods. The corresponding closed-loop responses also exhibit less oscillatory angle and position behavior. These findings indicate that SMA provides a more reliable and consistent FOPID tuning performance than GWO and AHA for the considered inverted pendulum problem.

Keywords: Inverted Pendulum Optimization, FOPID, SMA, AHA, GWO

Araba Üzerindeki Ters Sarkaç Sistemi için SMA Tabanlı Optimize Edilmiş FOPID Denetleyicisinin Karşılaştırmalı Performans Analizi

Öz

Bu çalışma, doğası gereği doğrusal olmayan ve kararsız bir sistem olan araba–ters sarkaç için Kesir Dereceli Oransal-İntegral-Türev (FOPID) kontrolörünün meta-sezgisel algoritmalar ile ayarlanmasını incelemektedir. Literatürde bu problem için çeşitli optimizasyon yöntemleri yaygın biçimde kullanılmakla birlikte, Cıvık Mantar Algoritması (SMA)'nın ters sarkaç kontrolündeki performansı yeterince araştırılmamıştır. Bu motivasyonla kontrolörün beş parametresi SMA, Gri Kurt Optimizasyonu (GWO) ve Yapay Sinek Kuşu Algoritması (AHA) kullanılarak belirlenmiş; tüm yöntemler özdeş benzetim koşulları altında Integral Zaman Mutlak Hata (ITAE) kriteri temelinde karşılaştırmalı olarak değerlendirilmiştir. Elde edilen sonuçlar, SMA tabanlı tasarımın diğer yöntemlere kıyasla daha düşük ITAE değişkenliği ve daha yüksek tekrarlanabilirlik sunduğunu göstermektedir. Buna karşılık gelen kapalı çevrim tepkileri de daha az salınımlı bir açı ve konum davranışı sergilemektedir. Bu bulgular, SMA'nın söz konusu problem için GWO ve AHA'ya kıyasla daha güvenilir ve tutarlı bir FOPID ayarlama performansı sağladığını ortaya koymaktadır.

Anahtar kelimeler: Ters Sarkaç, Optimizasyon, FOPID, SMA, AHA, GWO

1. INTRODUCTION

The inverted pendulum represents one of the most frequently studied platforms in control engineering, largely due to its ability to capture the essential dynamic characteristics observed in numerous real-world applications. As a canonical underactuated system, it possesses fewer actuating inputs than controllable degrees of freedom, a configuration commonly encountered across robotic and automation domains [1]. From a structural standpoint, the system operates as a single-input multiple-output (SIMO) arrangement, whereby a single horizontal force serves as the control input while both the cart displacement and the pendulum angle constitute the measured outputs. A further defining feature of this system is its inherently unstable and nonlinear behavior [2], which renders it a particularly valuable testbed for assessing the validity and effectiveness of control strategies. The literature documents a broad spectrum of mechanical configurations built upon this concept, including the double inverted pendulum [3], the rotational single-arm pendulum [4], and the cart–pendulum arrangement [5]. Control objectives associated with the inverted pendulum are generally grouped into three categories: swing-up control which seeks to bring the pendulum from its downward resting position to the upright configuration [6-7]; stabilization control, which maintains the pendulum in balance around the upright equilibrium [8-10]; and tracking control, which enables the system to follow a prescribed position trajectory while preserving stability [11-12]. Of these, stabilization and tracking are considered most relevant in practical implementations. A diverse set of control methodologies has been explored for the inverted pendulum over the years. Among conventional approaches, linear quadratic regulator (LQR)-based designs [13], standard PID controllers, and extended variants such as PI–PD structures [14-16] have all received considerable attention. Intelligent techniques, including fuzzy logic systems and neural network-based controllers, have similarly been applied to account for the system's nonlinear characteristics [17-18]. The FOPID controller, originally proposed by Podlubny, constitutes a generalization of the conventional PID architecture through the introduction of non-integer orders for both the integration and differentiation actions. Despite the long-standing mathematical foundations of fractional calculus, its engineering application was historically constrained by computational limitations. Growing computational capacity has since revitalized interest in fractional-order control, owing to the enhanced design flexibility and improved closed-loop performance it affords [19-21]. Numerous recent investigations have confirmed that FOPID controllers can surpass their integer-order counterparts across a variety of control scenarios [22-26], providing strong motivation for their adoption in this work. The FOPID controller is governed by five tuning variables (proportional, integral, and derivative gains together with the fractional integration and differentiation orders) each of which exerts a meaningful influence on the resulting closed-loop dynamics. Selecting appropriate values for these parameters is at least as consequential as choosing the controller structure itself. Conventional tuning strategies frequently prove inadequate when applied to inherently nonlinear systems such as the inverted pendulum. As a result, metaheuristic optimization algorithms have attracted growing interest owing to their capacity to handle complex, non-convex search landscapes efficiently [27-30]. These algorithms span a wide variety of design philosophies, encompassing biology-inspired, swarm-based, physics-based, and mathematics-derived paradigms. Despite this diversity, no universally superior method exists, which continues to drive the development of novel optimization techniques. Several researchers have investigated FOPID tuning for inverted pendulum systems. Mishra and Chandra [31] applied Particle Swarm Optimization (PSO) for this purpose, Lanjewar et al. [32] conducted a comparative study of dual-loop PID and FOPID controllers tuned via dynamic PSO, and Erkol [33] reported improved performance on a two-wheeled inverted pendulum using the artificial bee colony algorithm. A survey of the existing literature reveals a clear preference for well-established methods such as PSO, GWO, and ABC. The Slime Mould Algorithm (SMA), however, despite having demonstrated competitive results across various engineering optimization tasks, has received comparatively limited attention in the specific context of inverted pendulum control. Given its favorable convergence properties and relatively recent emergence, SMA constitutes a compelling candidate for this application. To enable a comprehensive performance comparison, GWO is included

CC: BY-NC-ND

as an established reference method because it is modeled on the social hierarchy and cooperative hunting strategies of grey wolves [34]. The Artificial Hummingbird Algorithm (AHA), introduced by Zhao et al. in 2022 and inspired by the foraging and hovering behaviors of hummingbirds, is additionally incorporated to represent a contemporary alternative metaheuristic [35–37].

Table 1. Summary of related studies on metaheuristic-based FOPID/PID tuning for inverted pendulum systems

Reference	Controller	Optimization	Plant / Objective	Main Limitation
Mishra and Chandra [31]	FOPID	PSO	Cart-IP / Frequency-domain	No time-domain metrics; single-run
Lanjewar et al. [32]	FOPID + LQR	Dynamic PSO	Rotary IP / Overshoot	No metaheuristic comparison; no ITAE
Erkol [33]	FOPID	ABC, PSO, GWO, CS	Two-wheeled IP / Error	Different platform; no simultaneous ITAE
Bhoi et al. [38]	FOPID	MGWO	Cart-IP / ITAE	Single algorithm; no multi-run statistics
Hasan et al. [39]	FOPI-FOPD	GWO	Rotary IP / ITSE	Rotary platform; no convergence analysis
Present Study	FOPID	SMA, GWO, AHA	Cart-IP (nonlinear) / ITAE +Time domain metrics	—

As summarized in Table 1, the existing studies predominantly employ PSO, GWO, or ABC for FOPID tuning, and none of the reviewed works applies SMA to the cart–inverted pendulum system using an ITAE-based FOPID tuning framework with separate time-domain evaluation of both pendulum angle and cart position. This gap motivates the present study. The present study conducts a comparative investigation of SMA, GWO, and AHA for tuning a FOPID controller applied to a cart–inverted pendulum system under identical simulation conditions. The findings offer a systematic assessment of SMA's suitability as an optimization tool within this control context, and simulation results confirm that the fractional-order controller achieves satisfactory simultaneous regulation of both cart position and pendulum angle in this nonlinear and inherently unstable system.

2. MATERIAL AND METHODS

2.1. Inverted Pendulum on Cart

Figure 1 depicts the fundamental configuration of the system, which includes a cart translating along the x-axis and a pendulum hinged at point P, allowing motion in the vertical plane. For effective control design, a comprehensive dynamic representation of the system must be formulated to capture both the cart translation and the pendulum rotation about its pivot. The governing equations are obtained based on classical mechanics principles. The configuration shown in Figure 1 comprises a cart of mass M and a pendulum of mass m with length l. All physical parameters utilized in the derivation of the system equations are listed in Table 2.

CC: BY-NC-ND

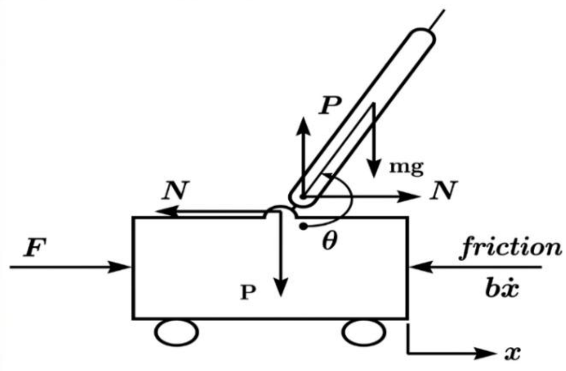

Figure 1. Inverted pendulum on cart.

Table 2. Parameters of the cart–inverted pendulum system

Parameter	**Description**	**Unit**
(M)	Mass of the cart	kg
(m)	Mass of the pendulum	kg
(F)	Applied thrust force	N
(l)	Length of the pendulum	m
(θ)	Pendulum angle from vertical axis	rad
(I)	Moment of inertia of the pendulum	$kg{\cdot}m^2$
(b)	Viscous friction coefficient of the cart	N.s/m

The basic equation of motion for a vehicle moving horizontally is;

$$F = M\ddot{x} + b\dot{x} + N \tag{1}$$

Sum of horizontal forces for the pendulum;

$$N = m\ddot{x} + ml\ddot{\theta}\cos\theta - ml\dot{\theta}^2\sin\theta \tag{2}$$

If equation (2) is substituted in equation (1), equation (3) is obtained.

$$F = (M + m)\ddot{x} + b\dot{x} + ml\ddot{\theta}\cos\theta - ml\dot{\theta}^2\sin\theta \tag{3}$$

To analyze the pendulum dynamics, the forces acting on the pendulum bob are resolved along the horizontal and vertical directions, yielding the moment equations about the pivot point given in Eqs. (4) and (5).

$$P\sin\theta + N\cos\theta - mg\sin\theta = ml\ddot{\theta} + m\ddot{x}\cos\theta \tag{4}$$

$$-Pl\sin\theta - Nl\cos\theta = I\ddot{\theta} \tag{5}$$

Equation (6) is obtained by combining Eqs. (4) and (5). Specifically, Eq. (5) is divided by l to express the reaction forces in terms of angular acceleration, and the resulting expression is added to Eq. (4). This operation eliminates the internal reaction forces P and N, and after rearranging and collecting terms, the rotational equation of motion for the pendulum is obtained as follows:

CC: BY-NC-ND

$$(\mathrm{I}+\mathrm{ml}^2)\ddot{\theta}+\mathrm{mglsin}\,\theta=-\mathrm{ml}\ddot{x}\cos\theta \tag{6}$$

In this study, the nonlinear equations of motion given in Eqs. (3) and (6) were used in the MATLAB/Simulink simulations. Therefore, the optimization process was carried out using the nonlinear time-domain responses of the cart–inverted pendulum system. The following linearized expressions are provided only for analytical completeness and to clarify the local dynamic relationship around the upright equilibrium.

$$\cos\theta=\cos(\pi+\varphi)\approx-1 \tag{7}$$

$$\sin\theta=\sin(\pi+\varphi)\approx-\varphi \tag{8}$$

$$\dot{\theta}^2=\dot{\varphi}^2\approx 0 \tag{9}$$

For the local linearized representation, substituting these approximations into Eqs. (3) and (6), the linearized equations of motion for the cart and pendulum are obtained as Eqs. (10) and (11), respectively.

$$(\mathrm{I}+\mathrm{ml}^2)\ddot{\varphi}-\mathrm{mgl}\varphi=\mathrm{ml}\ddot{x} \tag{10}$$

$$(\mathrm{M}+\mathrm{m})\ddot{x}+\mathrm{b}\dot{x}-\mathrm{ml}\ddot{\varphi}=\mathrm{u} \tag{11}$$

Applying the Laplace transform to Eqs. (10) and (11) under zero initial conditions yields the algebraic equations in the s-domain given in Eqs. (12) and (13). For the local linearized representation, the pendulum-angle transfer function with respect to the input force can be expressed as:

$$(\mathrm{I}+\mathrm{ml}^2)\Phi(\mathrm{s})\mathrm{s}^2-\mathrm{mgl}\Phi(\mathrm{s})=\mathrm{mlX}(\mathrm{s})\mathrm{s}^2 \tag{12}$$

$$(\mathrm{M}+\mathrm{m})\mathrm{X}(\mathrm{s})\mathrm{s}^2+\mathrm{bX}(\mathrm{s})\mathrm{s}-\mathrm{ml}\Phi(\mathrm{s})\mathrm{s}^2=\mathrm{U}(\mathrm{s}) \tag{13}$$

By eliminating X(s) from Eqs. (12) and (13), the pendulum-angle transfer function with respect to the input force is obtained as follows:

$$\frac{\Phi(\mathrm{s})}{U(s)}=\frac{\frac{ml}{q}s}{\mathrm{s}^3+\frac{b(I+m\mathrm{l}^2)}{q}\mathrm{s}^2-\frac{(M+m)mgl}{q}s-\frac{bmgl}{q}} \tag{14}$$

where q= $(\mathrm{M}+\mathrm{m})(\mathrm{I}+(ml^2))-(ml)^2$ is the common denominator term obtained from the determinant of the coupled linearized cart–pendulum equations. Here, (M) denotes the cart mass, (m) denotes the pendulum mass, (l) denotes the pendulum length, and (I) denotes the moment of inertia of the pendulum.

The numerical values of the cart–inverted pendulum parameters are listed in Table 3, and the corresponding MATLAB/Simulink model is presented in Figure 2.

CC: BY-NC-ND

Table 3. Numerical values of the cart–inverted pendulum system parameters

Parameter	Value
(M)	1 kg
(m)	0.5 kg
(l)	0.1 m
(I)	0.006 kg·m^2
(b)	0.1 N·s/m

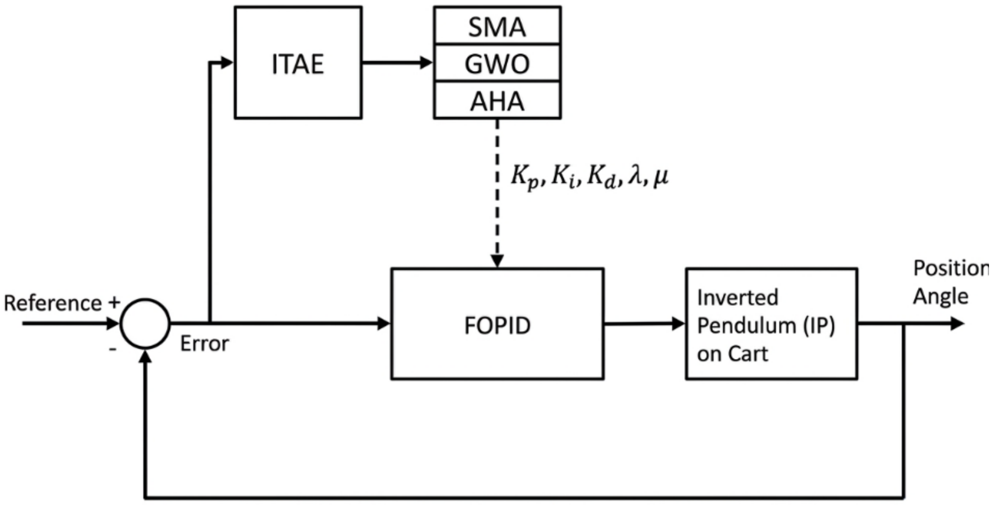

Figure 2. MATLAB/Simulink block diagram of the FOPID-controlled cart–inverted pendulum system.

In this block diagram, the FOPID controller is driven by the pendulum-angle error, and its output is applied as the horizontal control force to the cart. The cart-position signal is monitored as a system output and used for additional time-domain performance evaluation.

2.2. Fractional- Order PID (FOPID) Controller

A fractional-order controller extends the classical PID structure by allowing the integral and derivative actions to take non-integer orders [19–23]. Accordingly, the FOPID controller is defined by five adjustable parameters: the proportional, integral, and derivative gains, together with the fractional integration and differentiation orders, λ and μ. This extended structure provides greater flexibility in shaping the dynamic response compared with conventional PID controllers [24–26,40]. In this study, a single FOPID controller is employed to stabilize the pendulum angle around the upright equilibrium. The controller input is the pendulum-angle error, and the controller output represents the horizontal force applied to the cart. During the optimization process, the FOPID parameters K_p, K_i, K_d, λ and μ are tuned by minimizing the ITAE value calculated from the pendulum-angle error. The cart-position response is not included as a separate weighted term in the objective function; instead, it is evaluated separately through time-domain performance metrics. The transfer function of the FOPID controller is given in Eq. (15).

CC: BY-NC-ND

$$G_{FOPID}(s) = K_p + \frac{K_i}{s^{\lambda}} + K_d s^{\mu} \qquad \lambda, \mu > 0 \tag{15}$$

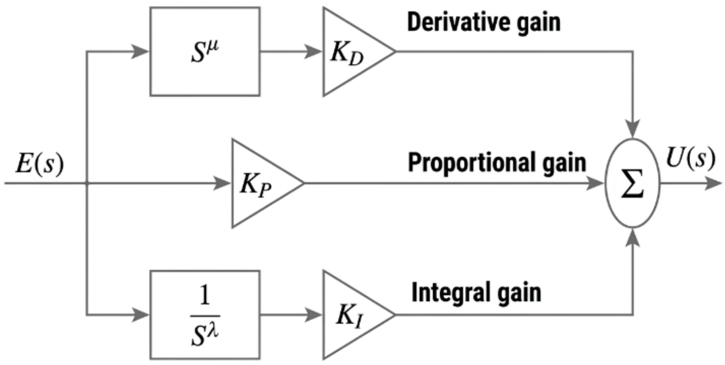

Figure 3. FOPID controller structure

Various approaches have been reported in the literature for determining the parameters of FOPID controllers. In the present study, these parameters were obtained using metaheuristic optimization algorithms. The FOPID controller was driven by the pendulum-angle error, while the cart-position response was monitored separately as an additional output of the system. In the FOPID controller, $s^{-\lambda}$ and s^{μ} represent the fractional integral and fractional derivative actions, respectively. Since these fractional-order terms cannot be implemented directly in Simulink, they were approximated using the Oustaloup recursive approximation method. In this study, an approximation order of 5 and a frequency range of [0.0001, 10] rad/s were used. The simulation was performed using a fixed-step ode3 (Bogacki–Shampine) solver with an automatic fixed-step size and a stop time of 10 s.

2.3. Slime Mould Algorithm (SMA)

The slime mould investigated in this work is mainly *Physarum polycephalum*, a unicellular eukaryotic organism that was historically misidentified as a fungus, giving rise to the term “slime mould.” Its developmental stages were systematically documented by Howard in 1931 [41]. This organism typically thrives in moist and low-temperature habitats. During nutrient-seeking activities, it extends toward nearby organic matter, surrounds the food source, and secretes enzymes to externally digest and subsequently absorb nutrients [42]. When confronted with multiple food sources of different qualities, *Physarum polycephalum* exhibits the ability to evaluate and preferentially move toward the most nutrient-rich option. Such behavior necessitates rapid yet adaptive decision-making to survive under uncertain environmental conditions. Empirical observations reveal an inverse relationship between decision speed and optimal choice probability, meaning that rapid decisions are often associated with lower selection reliability. This biological phenomenon reveals an intrinsic balance between environmental exploration and resource exploitation. The dynamic and adaptive foraging mechanism of the slime mould has inspired the formulation of bio-inspired optimization algorithms. Accordingly, SMA abstracts these biological nutrient-searching mechanisms into a mathematical model, facilitating effective navigation of complex, nonlinear, and multimodal search spaces.

CC: BY-NC-ND

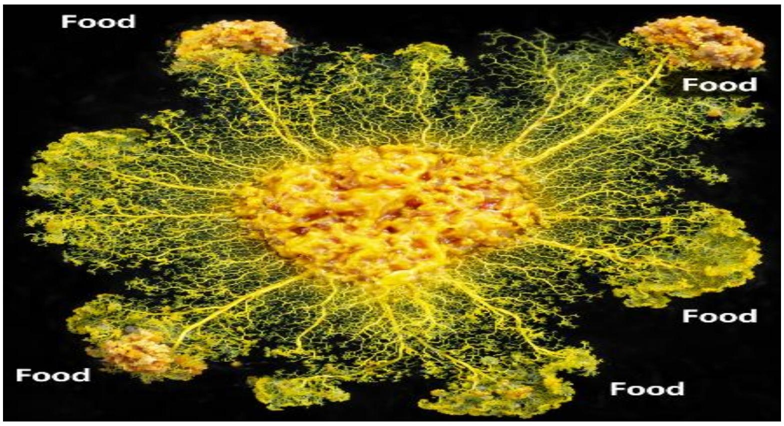

Figure 4. Foraging morphology of slime mould [43]

2.3.1 Approach Food

The slime mould senses surrounding food sources primarily through chemical cues dispersed in the air, commonly referred to as odor or concentration gradients. These chemical gradients act as regulatory mechanisms that steer the organism toward favorable regions. Variations in odor intensity provide spatial information that guides the slime mould toward regions with higher nutrient concentration. By continuously responding to these gradients, the slime mould is able to adjust its movement toward more favorable areas.

This directed motion is realized through rhythmic contraction and relaxation processes occurring within the body of the slime mould. Such contractions regulate cytoplasmic streaming, which in turn enables the organism to progress in a specific direction. Through this contraction-based mechanism, the slime mould exhibits an adaptive foraging behavior, allowing it to efficiently approach food sources while responding to environmental changes. This biologically driven contraction process constitutes a fundamental aspect of the slime mould's adaptive search strategy.

In order to utilize this behavior within optimization frameworks, the contraction-based movement of the slime mould can be represented using a mathematical model. Accordingly, the contraction mode that governs the slime mould's approach toward food sources is formulated mathematically as presented below.

$$\overrightarrow{X(t+1)} = \begin{cases} \overrightarrow{X_b}(t) + \overrightarrow{v_b} \cdot \left(\overrightarrow{(W)} \cdot \overrightarrow{X_A}(t) - \overrightarrow{X_B}(t) \right), r < p \\ \overrightarrow{v_c} \cdot \vec{X}(t), r \geq p \end{cases} \tag{16}$$

where $\overrightarrow{v_b}$ s a random parameter in the interval [-a a] and $\overrightarrow{v_c}$, linear decrease linearly from 1 to 0.

$\overrightarrow{X_b}(t)$ denotes the best position found so far t is the current iteration number, and r is a random number in the interval [0,1]. $X(t+1)$ represents the updated position of the slime mould. $X_A(t)$ and $X_B(t)$ denote the positions of two randomly selected individuals from the population.

$\overrightarrow{X(t+1)}$ = The next position taken by the slime mould.

$\overrightarrow{X_A}(t)$ ve $\overrightarrow{X_B}(t)$= Vectors containing the positions of two individuals randomly selected from the population.

The formula of p is as follows: p=tanh|S(i)-DF||

where i ∈ 1, 2, . . . , n, S(i) DF represents the best fitness obtained in all iterations, represents the fitness of $\vec{X}$.

CC: BY-NC-ND

$$\alpha = \operatorname{arctanh}(-(t/max\_t) + 1) \tag{17}$$

max_t = Maximum iteration number.

$\vec{W}$ weight of the slime mould and the formula for $\vec{W}$ is expressed as follows:

$$\overrightarrow{W(SmellIndex(i)} = \begin{cases} 1 + r.\log\left(\dfrac{bF - S(i)}{bF - wF} + 1\right), conditions \\ 1 - r.\log\left(\dfrac{bF - S(i)}{bF - wF} + 1\right), others \end{cases} \tag{18}$$

$$\text{SmellIndex} = \text{sort}(S) \tag{19}$$

Here, bF and wF denote the best and worst fitness values in the current iteration, respectively, and SmellIndex represents the ascending order of the fitness values for a minimization problem.

2.3.2 Wrap Food

This section formulates a mathematical representation of the contraction behavior observed in the venous tissue structure of the slime mould during the foraging process. The wave mechanism generated by the bio-oscillator within the organism directly influences the velocity of cytoplasmic streaming and, consequently, the thickness of the venous network. As the concentration of the encountered food source increases, the amplitude of the oscillatory wave produced by the bio-oscillator intensifies, resulting in accelerated cytoplasmic flow and reinforced vein structures.This interaction indicates the presence of a bidirectional feedback mechanism between the explored food concentration and the vein width of the slime mould. Equation (18) quantitatively describes this positive and negative feedback relationship. In regions where the food concentration is high, the corresponding weight assigned to that region is increased, thereby promoting local exploitation. Conversely, in areas with low food concentration, the assigned weight is reduced, encouraging exploration of alternative regions within the search space. Through this adaptive weighting strategy, a dynamic balance between exploration and exploitation is maintained throughout the search process. Based on this biologically inspired feedback mechanism, the mathematical model transforms the foraging behavior of the slime mould into an iterative numerical update rule. Considering the aforementioned factors, the mathematical expression governing the position update of the slime mould is presented below.

$$\overrightarrow{X^*} = \begin{cases} rand.(UB - LB) + LB, rand < z \\ \overrightarrow{X_b(t)} + \overrightarrow{v_b}.\left(W.\overrightarrow{X_A(t)} - \overrightarrow{X_B(t)}\right), \quad r < p \\ \overrightarrow{v_c}.\overrightarrow{X(t)}, r \geq p \end{cases} \tag{20}$$

UB and LB denote the upper and lower limits of the problem's search domain, respectively, whereas r and rand are random numbers generated within the interval [0,1]. In this formulation, z is defined as a probability parameter that determines whether SMA explores a new food source or performs a local search around the current best source [43].

The pseudo code of the algorithm is given in Algorithm 1.

Input: Objective function f(·), population size n, lower and upper bounds (lb, ub),

maximum number of iterations MaxIt

Output: BestX, BestF

Randomly generate an initial population Xi (i = 1, 2, ..., n) within [lb, ub]

CC: BY-NC-ND

Evaluate the fitness of each Xi

Determine the initial BestX and BestF

t = 1

while t ≤ MaxIt do

  Sort the population based on fitness values

  Update the adaptive control parameters

  for each search agent i do

    Update the position Xi according to the SMA update mechanism

    Apply boundary constraints to Xi

    Evaluate the fitness value of Xi

    if the new fitness improves BestF then

      Update BestF and BestX

    end if

  end for

  t = t + 1

end while

return BestX, BestF

Algorithm 1. Pseudo code of SMA

3. RESULTS AND DISCUSSION

Inverted pendulum system was implemented in the MATLAB/Simulink environment using the derived mathematical model. To evaluate the behavior of the considered optimization algorithms under different settings, two case studies were carried out by changing the population size and the maximum number of iterations. In both cases, the controller parameters were tuned using SMA, GWO, and AHA, and the obtained results were compared in terms of time-domain responses and ITAE values. The objective function used in the optimization process was defined as an ITAE criterion calculated from the pendulum-angle error signal in the Simulink model. The cart-position response was not included as a separate weighted term in the objective function; instead, it was evaluated separately using time-domain performance metrics. Accordingly, the ITAE objective function was formulated as: $J = \int_0^T t|\mathrm{e\theta}(t)|\mathrm{dt}$, where $\mathrm{e\theta}(t)$ denotes the pendulum-angle error and T represents the total simulation time. In the implemented Simulink model, the absolute value of this error signal was multiplied by simulation time and then integrated over the simulation interval. The pendulum angle and cart position responses were then evaluated separately using time-domain performance metrics. The simulation duration was selected as T=10 s. The parameter bounds were set as K_p, K_i, $K_d \in [0, 50]$ and λ, μ ∈ [0, 2] for all three algorithms. Ten independent optimization runs were performed for each algorithm in each case study, and both the descriptive statistics and statistical significance tests were based on these 10-run ITAE distributions. The Kruskal–Wallis test applied to the 10-run ITAE distributions yielded p=0.0009 for Case Study 1, indicating a statistically significant difference among the three algorithms. Pairwise Mann–Whitney U tests revealed that SMA-FOPID significantly outperformed AHA-FOPID (p=0.0002), and GWO-FOPID significantly outperformed AHA-FOPID (p=0.014), while no significant difference was found between SMA-FOPID and GWO-FOPID in terms of median performance (p=0.385). For Case Study 2, the Kruskal–Wallis test yielded p=0.412, and no significant pairwise differences were detected. Notably, GWO-FOPID produced an extreme outlier run

CC: BY-NC-ND

in Case Study 2, with a worst-case ITAE value of 4563.0547. Although the Kruskal–Wallis test did not indicate a statistically significant difference among the algorithms in Case Study 2, this outlier substantially increased the mean and standard deviation of GWO-FOPID. Therefore, the results should not be interpreted as statistically proven superiority of SMA-FOPID in median performance. Instead, they indicate that SMA-FOPID provides a more consistent tuning behavior with lower variability and better worst-case performance under the tested conditions.

3.1 Case Study 1

For the first experimental scenario, the integer-order gains K_p, K_i and K_d were constrained to the interval [0, 50], while the fractional differentiation and integration orders λ and μ were limited to [0, 2]. To ensure methodological consistency among the three metaheuristic strategies, identical population and iteration values (20 agents and 50 iterations) were employed. The internal control parameters of SMA, GWO, and AHA are summarized in Table 4. These selections were made to promote a stable balance between search diversification and intensification without imposing excessive computational burden. The corresponding dynamic responses of pendulum angle and cart displacement under the defined initial conditions are presented in Figures 5 and 6.

Table 4. Controller parameters of the metaheuristic algorithms

Algorithm	Population size	Iterations	Parameter	Value / Range
SMA	20	50	z	0.03
GWO	20	50	a	2 → 0
AHA	20	50	r	[0-1]

Here, z denotes the motion control parameter in SMA; a represents the coefficient that regulates the exploration–exploitation balance in GWO; and r refers to the random vector that determines the movement of search agents in AHA.

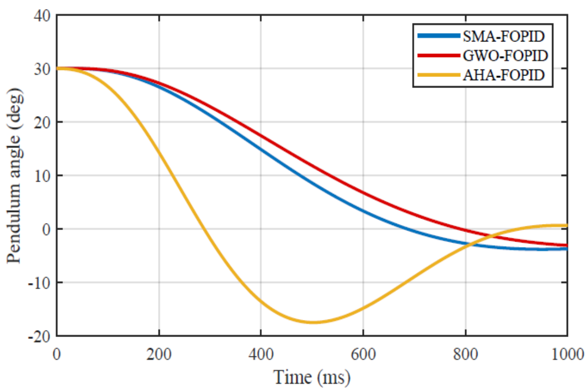

Figure 5. Pendulum angle response for Case Study 1 (initial angle: 30°, simulation duration: 10 s); comparison of SMA-FOPID, GWO-FOPID and AHA-FOPID controllers. Time axis restricted to 0–1000 ms to highlight transient behavior.

CC: BY-NC-ND

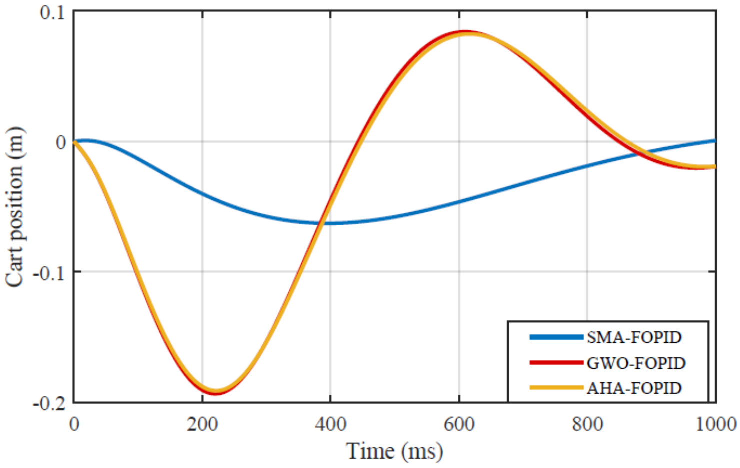

Figure 6. Cart position response for Case Study 1 (initial angle: 30°, simulation duration: 10 s); comparison of SMA-FOPID, GWO-FOPID and AHA-FOPID controllers.

Stable operation around the upright equilibrium requires simultaneous regulation of the pendulum angle and cart position. As illustrated in Figure 5, the SMA-tuned FOPID controller provides a smoother and more gradual angular response compared with the AHA-based design. Although GWO-FOPID exhibits a slightly lower overshoot and shorter settling time in this case, SMA-FOPID achieves a more balanced response when the ITAE variability, cart-position deviation, and control effort are considered together. Since upright stabilization corresponds to a zero-angle reference, reducing oscillatory behavior around this point remains an important performance indicator.

Table 5. The obtained fitness function values and controller parameters

ITAE					**Best Controller Parameters**				
Algorithm	**Best**	**Worst**	**Average**	**Standard deviation**	K_p	K_i	K_d	**λ**	**μ**
GWO-FOPID	6.7156	11.8761	8.7481	2.3025	0.0074	0.0035	0.0356	0.0844	0.9686
SMA-FOPID	5.5109	6.0613	5.9430	0.2136	0.0129	0.0010	0.0385	0.0010	1.0078
AHA-FOPID	6.1875	10.7462	8.4639	1.9677	0.2583	0.0013	0.2453	0.0253	1.6461

Table 5 shows that SMA-FOPID achieves the lowest best, worst, average, and standard deviation values among the compared algorithms in Case Study 1. This indicates that the SMA-based tuning process provides not only better average ITAE performance but also a more consistent distribution across repeated runs. The optimized SMA-FOPID parameters are generally small in magnitude, particularly K_i and K_d, suggesting that effective stabilization can be achieved without aggressive integral or derivative action. In contrast, AHA-FOPID employs considerably larger K_p and K_d values, which is consistent with the higher overshoot observed in the time-domain response. The fractional-order parameters λ and μ further shape the memory and dynamic characteristics of the controller, allowing the optimization process to balance transient response and stability without manual tuning. Finally, a comparative evaluation of the optimization algorithms based on the ITAE metric is presented in Figure 7, illustrating the more consistent convergence behavior of the SMA-FOPID approach.

CC: BY-NC-ND

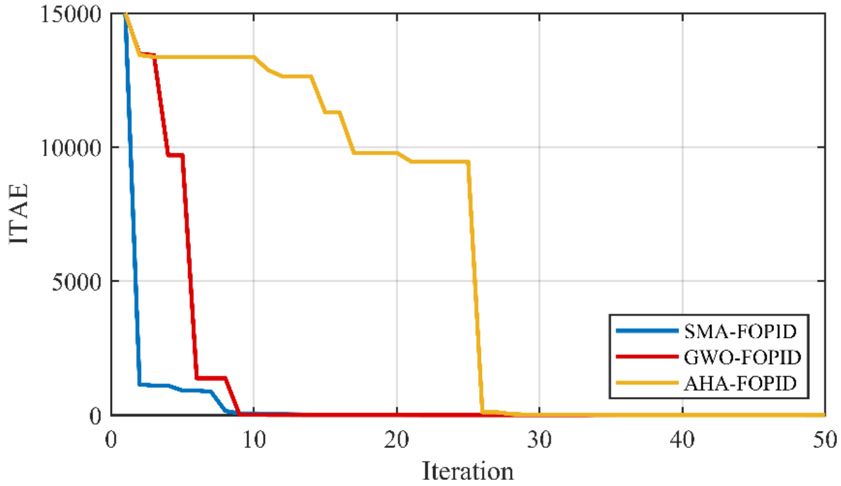

Figure 7. Convergence curves of the optimization algorithms for Case Study 1 (20 agents, 50 iterations); best run selected from 10 independent trials.

The convergence behavior shown in Figure 7 indicates that SMA and GWO achieve similar best-case ITAE values. However, the significantly lower standard deviation of SMA reported in Table 5 demonstrates more consistent optimization performance, leading to improved robustness in control design.

Table 6. Time-domain performance metrics for Case Study 1 (initial angle: 30°)

Algorithm	**Overshoot (%)**	**Settling Time (s)**	**Rise Time (s)**	**SS Angle Error (°)**	**Max Angle Dev. (°)**	**Max Cart Pos. Dev. (m)**	**Peak Control Force (N)**	**Control Effort ($N^2.s$)**
SMA-FOPID	26.999	1.922	0.418	0.0032	30.006	0.637	4.681	5.030
GWO-FOPID	45.597	1.645	0.484	0.5122	30.006	1.122	9.012	26.127
AHA-FOPID	58.59	2.029	0.175	2.93×10^{-6}	30.000	1.646	16.238	61.051

Time-domain and additional performance metrics for Case Study 1 are summarized in Table 6. Although GWO-FOPID achieves a slightly faster settling time (1.645 s), SMA-FOPID demonstrates superior consistency across repeated runs as evidenced by its significantly lower standard deviation in Table 5. AHA-FOPID exhibits the fastest rise time (0.175 s) but at the cost of an overshoot exceeding 58%, which is unacceptable in precision stabilization tasks. In terms of steady-state angle error, SMA-FOPID yields a value of 0.0032°, which is substantially lower than that of GWO-FOPID (0.5122°), indicating more accurate regulation around the upright equilibrium. The maximum cart position deviation of SMA-FOPID (0.637 m) is also considerably smaller than those of GWO-FOPID (1.122 m) and AHA-FOPID (1.646 m), reflecting a more restrained transient response. Furthermore, SMA-FOPID requires significantly lower peak control force (4.681 N) and control effort (5.030 N^2·s) compared with GWO-FOPID (9.012 N, 26.127 N^2·s) and AHA-FOPID (16.238 N, 61.051 N^2·s), demonstrating that the SMA-tuned controller achieves effective stabilization with considerably lower actuation demand. The control effort was calculated as $\int_0^T u^2(t)dt$, where u(t) denotes the control force applied to the cart.

CC: BY-NC-ND

3.2 Case Study 2

In Case Study 2, the K_p, K_i, and K_d were selected within the range of 0 to 50, consistent with the parameter limits adopted in Case Study 1. The fractional-order parameters λ and μ were constrained to the interval [0, 2], ensuring physically meaningful controller behavior. To enhance the exploration capability of the optimization process, the population size was increased to 50, while the number of iterations was set to 100 for each of the three algorithms. This configuration allows a broader search of the solution space and improves the reliability of the optimization results, particularly in more complex or nonlinear regions of the search domain. In the SMA, the control parameter z was again fixed at 0.03, maintaining consistency with the previous case study and enabling a fair comparison of algorithmic performance under different population settings. Under the specified initial conditions, the resulting angle and position responses of the inverted pendulum system are illustrated in Figures 8 and 9, respectively.

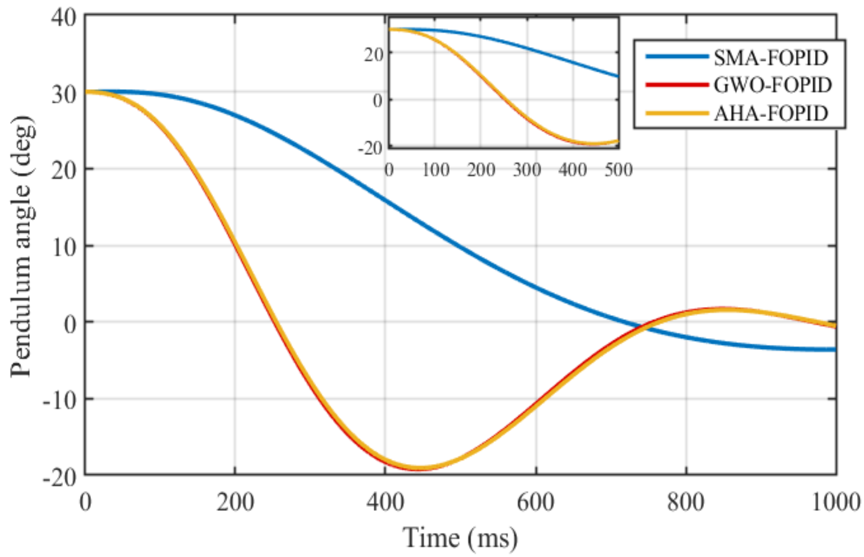

Figure 8. Pendulum angle response for Case Study 2 (initial angle: 30°, simulation duration: 10 s); comparison of SMA-FOPID, GWO-FOPID and AHA-FOPID controllers. Inset shows zoomed view (0–500 ms, −25° to 30°).

As shown in Figure 8, SMA-FOPID and GWO-FOPID exhibit relatively comparable best-run angular responses in Case Study 2, whereas AHA-FOPID shows a faster but more aggressive transient behavior. Although AHA-FOPID reaches the reference region rapidly, this response is accompanied by a considerably higher overshoot and larger control effort, as also confirmed by the quantitative results in Table 7. In contrast, SMA-FOPID provides a smoother and more balanced response with low oscillation and reduced control effort. In terms of cart-position response, SMA-FOPID and GWO-FOPID exhibit relatively close deviation levels, whereas AHA-FOPID produces a considerably larger cart-position excursion. This result is consistent with the higher overshoot and control effort values reported in Table 7. Conversely, the SMA-FOPID controller ensures a more gradual and stable convergence to the reference trajectory, with noticeably attenuated oscillations during the transient interval. The observed discrepancies in response characteristics stem from the distinct parameter distributions generated by each optimization strategy. Table 8 presents the controller parameters and the corresponding ITAE values obtained for Case Study 2. An examination of the table shows that the GWO-FOPID, SMA-FOPID, and AHA-FOPID approaches exhibit distinct behaviors in terms of ITAE performance and parameter distributions. Although GWO-FOPID yields a competitive best ITAE value, it is accompanied by a considerably large worst value and standard deviation, indicating a high level of variability in the obtained results. In contrast, SMA-FOPID produces consistently lower and closely clustered ITAE values, as reflected by both its average performance and the smallest standard

CC: BY-NC-ND

deviation among the considered algorithms, suggesting improved stability and robustness. The AHA-FOPID approach demonstrates a narrower dispersion of ITAE values compared to GWO-FOPID; however, its average performance and variability remain higher than those achieved by SMA-FOPID. An analysis of the optimized controller parameters further reveals that each algorithm converges toward different gain values and fractional orders, reflecting the influence of their respective search strategies on the resulting controller configurations. The evaluation based on the ITAE criterion is further supported by the comparison of objective function values illustrated in Figure 10. Overall, the results indicate that the SMA-FOPID approach provides a more balanced trade-off between performance and consistency compared to the other methods considered.

Table 7. Time-domain performance metrics for Case Study 2 (initial angle: 30°)

Algorithm	**Overshoot (%)**	**Settling Time (s)**	**Rise Time (s)**	**SS Angle Error (°)**	**Max Angle Dev. (°)**	**Max Cart Pos. Dev. (m)**	**Peak Control Force (N)**	**Control Effort ($N^2.s$)**
SMA-FOPID	33.178	1.907	0.437	0.0040	30.015	0.626	4.592	4.847
GWO-FOPID	30.621	1.891	0.436	0.0061	30.006	0.628	4.598	4.851
AHA-FOPID	63.64	1.809	0.154	4.23×10^{-5}	30.000	1.909	20.325	97.428

As shown in Table 7, SMA-FOPID and GWO-FOPID exhibit nearly identical overshoot and settling time values in Case Study 2. However, GWO-FOPID yields a worst-case ITAE value of 4563.0547 in the extended 10-run analysis (Table 8), indicating that some runs converge to highly suboptimal or unstable solutions, possibly due to premature convergence caused by loss of population diversity. AHA-FOPID again achieves the fastest rise time (0.154 s), but this is accompanied by an overshoot exceeding 63%, which indicates an aggressive transient behavior. Overall, SMA-FOPID delivers competitive time-domain performance with lower variability, suggesting a more consistent tuning behavior under the tested conditions.

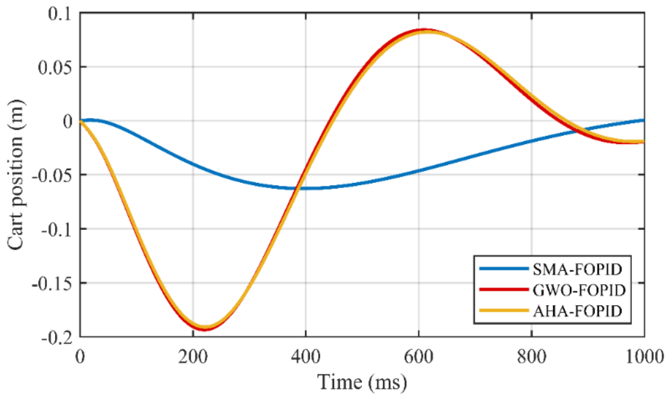

Figure 9. Cart position response for Case Study 2 (initial angle: 30°, simulation duration: 10 s); comparison of SMA-FOPID, GWO-FOPID and AHA-FOPID controllers.

CC: BY-NC-ND

Table 8. The obtained fitness function values and controller parameters

ITAE					Best Controller Parameters				
Algorithm	**Best**	**Worst**	**Average**	**Standard deviation**	K_p	K_i	K_d	λ	μ
GWO-FOPID	6.0447	4563.0547	917.2515	2038.0659	0.0122	0.0011	0.0382	0.0534	1.0037
SMA-FOPID	5.7188	6.0666	5.9866	0.1499	0.0010	0.0129	0.0388	0.0010	1.0076
AHA-FOPID	5.9703	6.4419	6.0811	0.2035	0.3401	0.0011	0.2569	0.0233	1.7892

The convergence curves shown in Figure 10 indicate that SMA-FOPID and GWO-FOPID exhibit similar decreasing trends in ITAE, with SMA-FOPID reaching low ITAE values at earlier iterations, reflecting faster convergence. AHA-FOPID, on the other hand, demonstrates delayed convergence, remaining at higher ITAE levels for a longer portion of the optimization process before a rapid reduction occurs. These convergence characteristics are consistent with the statistical results reported in Table 8. In particular, SMA-FOPID produces ITAE values within a narrow range, as reflected by its low standard deviation, whereas GWO-FOPID exhibits substantial variability and AHA-FOPID shows moderate dispersion. Together, the convergence behavior and statistical distribution of ITAE values highlight clear differences in the optimization dynamics of the algorithms under identical population and iteration settings.

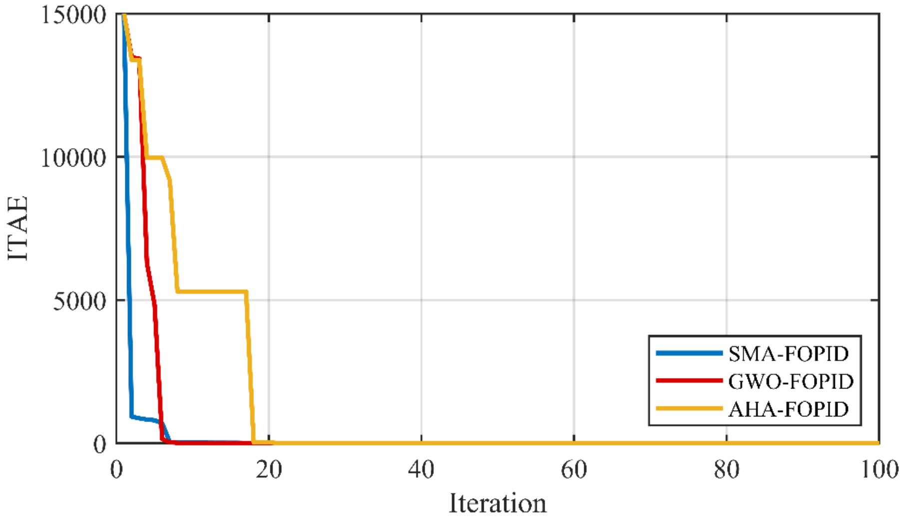

Figure 10. Convergence curves of the optimization algorithms for Case Study 2 (50 agents, 100 iterations); best run selected from 10 independent trials.

3.3. Baseline Comparison

To assess the contribution of the fractional-order controller structure under the same optimizer, a classical PID controller (λ=1, μ=1) was tuned using SMA under the same conditions as Case Study 1. The SMA-tuned PID controller yielded a best ITAE value of 12.54, compared to 5.5109 for SMA-FOPID, corresponding to approximately a 56.1% improvement. Figure 11 illustrates the time-domain responses of SMA-FOPID and SMA-PID. These results indicate that the fractional-order terms λ and μ contribute meaningfully to the improved control performance.

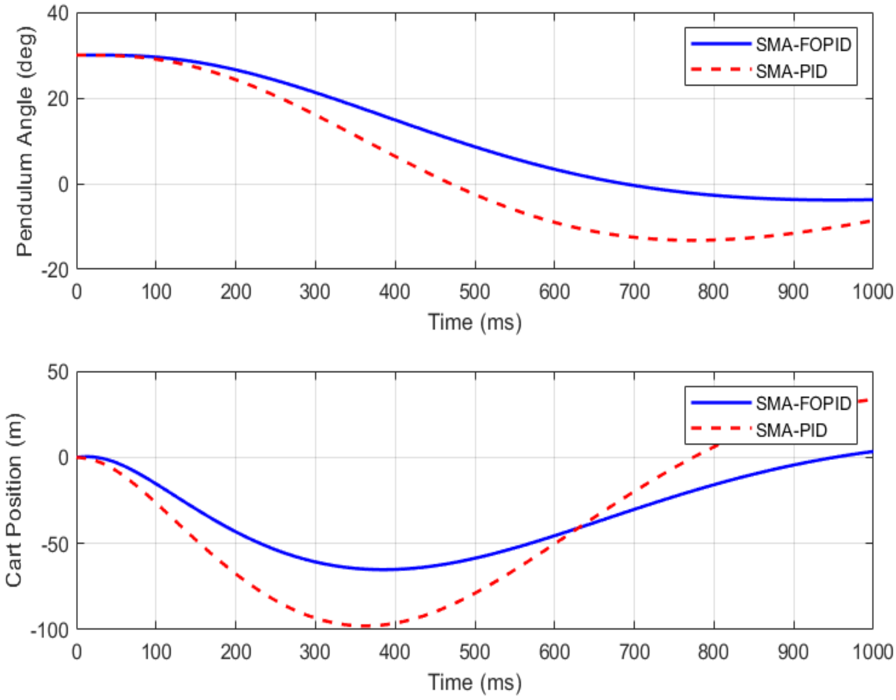

Figure 11. Time-domain response comparison of SMA-FOPID and SMA-PID controllers (initial angle: 30°, simulation duration: 10 s, Case Study 1 parameters).

3.4 Robustness Analysis

To further evaluate the generalization capability of the proposed SMA-FOPID controller, a robustness analysis was conducted by testing all three controllers under different initial pendulum angles: 15°, 30°, and 45°. The best controller parameters obtained from Case Study 1 were used without re-tuning, in order to assess how well each controller maintains performance under varying initial conditions. The settling times of the pendulum angle response for each algorithm and initial angle are summarized in Table 9. Settling time was defined as the last time instant at which the pendulum angle exceeded a 2% tolerance band of the initial displacement.

Table 9. Settling times (s) of pendulum angle under different initial conditions.

Algorithm	**15° (s)**	**30° (s)**	**45° (s)**
SMA-FOPID	3.488	1.922	1.922
GWO-FOPID	3.664	1.645	5.651
AHA-FOPID	2.000	2.029	2.048

As shown in Table 9, SMA-FOPID exhibits identical settling times of 1.922 s at both 30° and 45°, indicating that its transient response remains stable when the initial pendulum angle is increased from 30° to 45°. GWO-FOPID achieves the fastest settling at 30° (1.645 s); however, its settling time increases considerably to 5.651 s at 45°, indicating sensitivity to larger initial-condition variations. AHA-FOPID maintains relatively uniform settling times between 2.000 s and 2.048 s; however, when considered together with the ITAE results and overshoot characteristics, its overall performance remains less favorable than SMA-FOPID. These results indicate that SMA-FOPID provides competitive and consistent transient performance under the tested initial-condition variations.

CC: BY-NC-ND

4. CONCLUSIONS

The performance of the algorithms was investigated on a cart–inverted pendulum system through two different case studies. The evaluation was carried out based on the ITAE performance index calculated from the pendulum-angle error, while the cart-position response was assessed separately using time-domain performance metrics. The results indicate that the SMA-based optimization approach provides more consistent controller tuning across repeated runs. In both case studies, SMA-FOPID exhibited a narrow ITAE distribution with a low standard deviation, whereas GWO-FOPID achieved competitive best-case results but showed higher variability in some runs. AHA-FOPID demonstrated a faster but more aggressive transient response, which was accompanied by increased overshoot and higher control effort.

The angle and cart-position responses support these observations. Although GWO-FOPID provided slightly faster settling in some cases, SMA-FOPID generally achieved a more balanced response when ITAE variability, cart-position deviation, peak control force, and control effort were considered together. The baseline comparison with SMA-PID further showed that the fractional-order controller structure contributed to the improved ITAE performance. In addition, the initial-condition analysis indicated that SMA-FOPID maintained competitive and consistent transient behavior under the tested angle variations.

Overall, the findings suggest that SMA is a promising optimization method for FOPID tuning in the cart–inverted pendulum control problem. Future work will focus on extending the proposed framework by considering additional operating conditions, disturbance inputs, parameter uncertainties, actuator saturation, and experimental validation.

Peer-review: External, Independent.

Acknowledgements:

-

Declarations:

1. Statement of Originality:

The authors declare that this manuscript is an original work, has not been published previously, and is not under consideration for publication elsewhere, either in whole or in part. All data, figures, and analyses presented are the authors' own work.

2. Author Contributions:

Concept: MT; ***Conceptualization:*** MT; ***Literature Search:*** MT; ***Data Collection:*** MT; ***Data Processing:*** MT; ***Analysis:*** MT; ***Writing – original draft:*** MT,HZ,SS; ***Writing – review & editing:*** MT,HZ,SS.

3. Ethics approval:

Not applicable.

4. Funding/Support:

This research received no specific grant from any funding agency in the public, commercial, or not-for-profit sectors.

5. Competing Interests:

The authors declare no competing interests.

6. GenAI Usage Statement:

No GenAI tools were used at any stage of the study.

7. Sustainable Development Goals:

☐ 1 NO POVERTY ☐ 2 ZERO HUNGER ☐ 3 GOOD HEALTH AND WELL-BEING ☐ 4 QUALITY EDUCATION ☐ 5 GENDER EQUALITY ☐ 6 CLEAN WATER AND SANITATION ☐ 7 AFFORDABLE AND CLEAN ENERGY

❋ ❋ ❋

REFERENCES

[1] Liu, Y. & Yu, H. (2013). A survey of underactuated mechanical systems. IET Control Theory and Applications, 7(7), 921–935.

[2] Furuta, K. (2003). Control of pendulum: From super mechano-system to human adaptive mechatronics. Proceedings of the 42nd IEEE International Conference on Decision and Control, Maui, HI, USA, 149–156.

[3] Li, Q. R., Tao, W. H., Sun, N., Zhang, C. Y. & Yao, L. H. (2008). Stabilization control of double inverted pendulum system. Proceedings of the 3rd International Conference on Innovative Computing, Information and Control, Dalian, China, 1–6.

[4] Åström, K. J. & Furuta, K. (2000). Swinging up a pendulum by energy control. Automatica, 36(2), 287–295.

[5] Yoshida, K. (1999). Swing-up control of an inverted pendulum by energy-based methods. Proceedings of the American Control Conference, San Diego, CA, USA, 4045–4049.

[6] Mason, P., Broucke, M. & Piccoli, B. (2008). Time optimal swing-up of the planar pendulum. IEEE Transactions on Automatic Control, 53(8), 1876–1886.

[7] Tao, C. W., Taur, J. S., Hsieh, T. W. & Tsai, C. L. (2008). Design of a fuzzy controller with fuzzy swing-up and parallel distributed pole assignment schemes for an inverted pendulum and cart system. IEEE Transactions on Control Systems Technology, 16(6), 1277–1288.

[8] Shahnazi, R. & Akbarzadeh-T, M. R. (2008). PI adaptive fuzzy control with large and fast disturbance rejection for a class of uncertain nonlinear systems. IEEE Transactions on Fuzzy Systems, 16(1), 187–197.

[9] Bloch, A. M., Leonard, N. E. & Marsden, J. E. (2000). Controlled Lagrangians and the stabilization of mechanical systems. I. The first matching theorem. IEEE Transactions on Automatic Control, 45(12), 2253–2270.

[10] Chaturvedi, N. A., McClamroch, N. H. & Bernstein, D. S. (2008). Stabilization of a 3D axially symmetric pendulum. Automatica, 44(9), 2258–2265.

[11] Wai, R. J. & Chang, L. J. (2006). Adaptive stabilizing and tracking control for a nonlinear inverted-pendulum system via sliding-mode technique. IEEE Transactions on Industrial Electronics, 53(2), 674–692.

[12] Chang, L. H. & Lee, A. C. (2007). Design of nonlinear controller for bi-axial inverted pendulum system. IET Control Theory and Applications, 1(4), 979–986.

[13] Wang, H., Dong, H., He, L., Shi, Y. & Zhang, Y. (2010). Design and simulation of LQR controller with the linear inverted pendulum. Proceedings of the International Conference on Electrical and Control Engineering, Wuhan, China, 1–4.

[14] Wang, J. J. (2011). Simulation studies of inverted pendulum based on PID controllers. Simulation Modelling Practice and Theory, 19(1), 440–449.

[15] Lim, Y. Y., Hoo, C. L. & Wong, Y. M. F. (2018). Stabilising an inverted pendulum with PID controller. MATEC Web of Conferences, 152, 03022.

[16] Peker, F. & Kaya, I. (2017). Identification and real-time control of an inverted pendulum using PI–PD controller. Proceedings of the 21st International Conference on System Theory, Control and Computing, Sinaia, Romania, 1–6.

[17] Elsayed, B. A., Hassan, M. A. & Mekhilef, S. (2015). Fuzzy swinging-up with sliding mode control for third-order cart–inverted pendulum system. International Journal of Control, Automation and Systems, 13(1), 238–248.

[18] Anderson, C. W. (1989). Learning to control an inverted pendulum using neural networks. IEEE Control Systems Magazine, 9(3), 31–37.

[19] Ortigueira, M. D. (2011). Fractional Calculus for Scientists and Engineers. Springer, Dordrecht, The Netherlands.

[20] Caponetto, R., Dongola, G., Fortuna, L. & Petráš, I. (2010). Fractional Order Systems: Modeling and Control Applications. World Scientific, Singapore.

[21] Baleanu, D., Diethelm, K., Scalas, E. & Trujillo, J. J. (2012). Fractional Calculus Models and Numerical Methods. World Scientific, Singapore.

[22] Podlubny, I. (1999). Fractional-order systems and PIλDμ controllers. IEEE Transactions on Automatic Control, 44(1), 208–214.

[23] Podlubny, I., Petráš, I., Vinagre, B. M., O'Leary, P. & Dorčák, Ľ. (2002). Analogue realizations of fractional-order controllers. Nonlinear Dynamics, 29(1–4), 281–296.

[24] Yeroglu, C. & Tan, N. (2011). Note on fractional-order proportional–integral–differential controller design. IET Control Theory and Applications, 5(17), 1978–1989.

[25] Maiti, D., Acharya, A., Chakraborty, M., Konar, A. & Janarthanan, R. (2008). Tuning PID and PI/λDδ controllers using the integral time absolute error criterion. Proceedings of the International Conference on Information and Automation for Sustainability, Colombo, Sri Lanka, 1–6.

[26] Das, S., Das, S. & Gupta, A. (2011). Fractional order modeling of a PHWR under step-back condition and control of its global power with a robust PIλDμ controller. IEEE Transactions on Nuclear Science, 58(5), 2431–2441.

[27] Chen, H., Wang, M., Li, S. & Mirjalili, S. (2019). An opposition-based sine cosine approach with local search for parameter estimation of photovoltaic models. Energy Conversion and Management, 195, 927–942.

[28] Chen, H., Xu, Y., Wang, M. & Zhao, X. (2019). A balanced whale optimization algorithm for constrained engineering design problems. Applied Mathematical Modelling, 71, 45–59.

[29] Wang, M. & Chen, H. (2020). Chaotic multi-swarm whale optimizer boosted support vector machine for medical diagnosis. Applied Soft Computing, 88, 105946.

[30] Wang, M., Chen, H., Li, S. & Mirjalili, S. (2017). Toward an optimal kernel extreme learning machine using a chaotic moth–flame optimization strategy. Neurocomputing, 267, 69–84.

[31] Mishra, S. K. & Chandra, D. (2014). Stabilization and tracking control of inverted pendulum using fractional-order PID controllers. Journal of Engineering, 2014, 752918.

[32] Lanjewar, A., Khubalkar, S. W. & Junghare, A. S. (2018). Comparative analysis of two-loop integer and fractional-order PID controller for inverted pendulum. Proceedings of the International Conference on Smart Electric Drives and Power Systems, Nagpur, India, 1–6.

[33] Erkol, H. O. (2018). Optimal PIλDμ controller design for two-wheeled inverted pendulum. IEEE

CC: BY-NC-ND

Access, 6, 75709–75717.

[34] Mirjalili, S., Mirjalili, S. M. & Lewis, A. (2014). Grey wolf optimizer. Advances in Engineering Software, 69, 46–61.

[35] Zhao, W., Wang, L. & Mirjalili, S. (2022). Artificial hummingbird algorithm: A new bio-inspired optimizer with its engineering applications. Computer Methods in Applied Mechanics and Engineering, 388, 114194.

[36] Soylu, S. (2024). Performance analysis of fractional-order controllers for blade pitch angle control of a wind turbine. Proceedings of the 4th International Conference on Electrical, Computer, Communications and Mechatronics Engineering (ICECCME), 1–6.

[37] Çelik, M. & Soylu, S. (2023). Parameter estimation study of polymer electrolyte membrane fuel cell using artificial hummingbird algorithm. Proceedings of the Institution of Mechanical Engineers, Part C, 237(8), 1956–1967.

[38] Bhoi, S., Rout, N. C., & Rout, B. C. (2017). MGWO meta heuristic algorithm vs. classical tuning method of FOPID controller for inverted pendulum. International Conference on Innovations in Control, Communication and Information Systems, 1–7.

[39] Hasan, M. A., Oglah, A. A., & Marie, M. J. (2023). Optimal FOPI-FOPD controller design for rotary inverted pendulum system using grey wolves' optimization technique. TELKOMNIKA Telecommunication Computing Electronics and Control, 21(3), 657–666.

[40] Shah, P. & Agashe, S. (2016). Review of fractional PID controller. Mechatronics, 38, 29–41.

[41] Howard, F. L. (1931). The life history of Physarum polycephalum. American Journal of Botany, 18(2), 116–133.

[42] Latty, T. & Beekman, M. (2010). Food quality and the risk of light exposure affect patch-choice decisions. Ecology, 91(1), 22–27.

[43] Li, S., Chen, H., Wang, M., Heidari, A. A. & Mirjalili, S. (2020). Slime mould algorithm: A new method for stochastic optimization. Future Generation Computer Systems, 111, 300–323.

CC: BY-NC-ND